High-power single-mode solid-state laser with a short, wide unstable cavity

Dmitrii Kouznetsov, Jean-François Bisson, Kazunori Takaichi, and Ken-ichi Ueda

Institute for Laser Science, University of Electro-Communications, 1-5-1 Chofu, Tokyo 182-8585, Japan

Received July 26, 2004; revised manuscript received February 4, 2005; accepted February 15, 2005

A wide, short unstable cavity laser design is proposed for high-power, single-longitudinal, single-transverse-mode emission from a solid-state laser. Such a laser combines the single-mode master oscillator and the single-mode amplifier in a single piece. Design formulas are suggested; the efficiency and conditions of the single-longitudinal-mode operation are analyzed. Examples with Nd:YAG and Yb:YAG are considered. For a device of a few millimeters wide, the slope efficiency of ≈50% and the threshold of a few watts are predicted. © 2005 Optical Society of America

OCIS codes: 140.3570, 140.3410, 140.3580, 080.2740, 140.3300, 140.3530.

1. INTRODUCTION

Several applications require the concentration of a high-power light source onto a small area. It can be important for two-photon microscopy, the study of highly relativistic laser–plasma interactions, and precise cutting in micromachining. This requires high-beam-quality, high-power laser sources. Some applications (laser frequency stabilization, interferometric gravitational-wave detection, or space communications) also require single-transversal-mode (STM) and single-longitudinal mode (SLM) operation. The STM operation is difficult to obtain at high power when stable cavities are used. The powerful sources of light emission sometimes combine a master oscillator with a power amplifier[1,2] or use unstable resonators.[3,4] Because of the relatively long length of resonators, these lasers emit many longitudinal modes. Achievement of SLM operation in solid-state lasers requires special efforts because the spatial hole burning (SHB) destabilizes the monochromatic standing wave.[5,6] The ring cavities,[7,8] twisting of modes,[9] or even the electro-optical modulation[10] allows for the avoidance of the SHB. Most of single-mode lasers use the longitudinal scheme of delivery of the pump. The mismatch of the pump beam and the signal mode leads to low efficiency of the device; typically, monolithic, isolated, single-mode, end-pumped ring oscillators[7] dissipate ≈100 W to yield a watt of single-mode output.

Here we propose a short unstable cavity that makes it possible to achieve both SLM and STM operation with high efficiency. It includes a master oscillator and amplifier integrated in the same device as shown in Fig. 1. The device consists of a pie-shaped unstable cavity with offset geometry, which provides STM oscillations, and input and output windows. The seed of laser oscillation takes place in the small region where the plano—convex mirrors facing each other are parallel. Some part of this seed signal leaks away from the seed region due to the convex reflecting surface and is then amplified without feedback, as in a single-pass amplifier.

Such a scheme also allows transversal delivery of the pump, similar to that considered in Ref. 11. Then the high absorption efficiency of the pump beam, required for the efficient operation of the device, can be combined with the short length of the resonator, required for SLM operation. The device shown in Fig. 1 has a flat bottom mirror that can be placed on a heat sink. A large surface for cooling allows power scaling. A large volume-to-length ratio may also be useful for the generation of energetic solitary pulses of high quality.

The pie-shaped device shown in Fig. 1 may be difficult to manufacture. The configuration shown in Fig. 2 should be easier to realize. The pump is still confined in the vertical direction. It should be focused to the optical axis of the unstable cavity. This focusing can partially compensate for the depletion of the pump because of the absorption in the active medium. Then the intensity will not vary by much on the right-hand side of the device. As for the left-hand side of the cavity, the already depleted pump beam diverges, so the gain should be weak. The shape of the pumped areas in Figs. 1 and 2 determines the direction and numerical aperture (NA) of the output signal in the horizontal direction. The length h of the amplifier (thickness of the specimen) and magnification coefficient M of the resonator determine the NA of the output signal in the vertical direction. An example of the signal ray tracing is shown in Fig. 3.

Recently, the tapered slab delivery of the pump to the active fiber[12–14] was suggested, which also provides an almost constant pump intensity along the fiber laser; the advantages of such a delivery were also discussed. Here we consider the solid-state analogy. We analyze the conditions when the intensities of both pump and signal remain approximately constant during the propagation of the pump from the input window to the seed region and propagation of the signal from the seed region to the output window.

In the standing-wave resonator, the single-mode operation is limited by the SHB.[5,6] This SHB can be mitigated with a special coating of the surface of a mirror with birefringent layers, which causes the twisting of

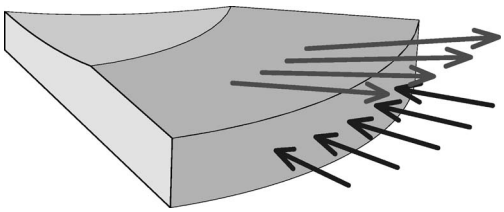

Fig. 1. Pie-shaped solid-state laser with an unstable cavity.

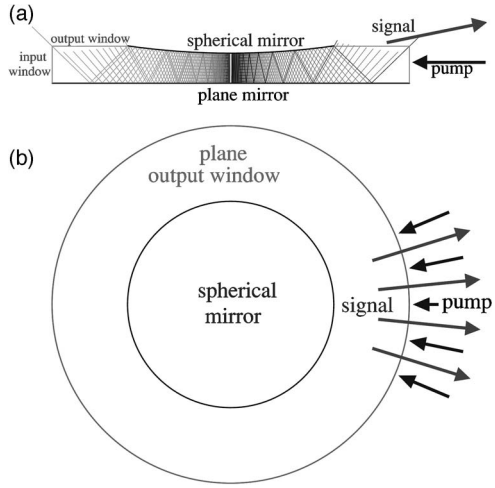

Fig. 2. (a) Rays of the signal in a laser with an unstable cavity pumped laterally; (b) the pie-shaped pumped region can be merged into a disk of an active medium.

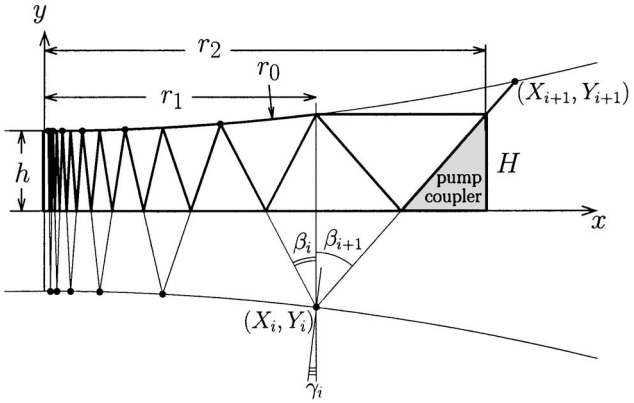

Fig. 3. Ray tracing in the unstable cavity and the resulting geometry of the device.

polarization[9] in such a way that the polarization of the wave going forward is orthogonal to that of the wave going backward. This technique can be applied to our device. However, the birefringent coating may be not suitable for the prototype of the device. Therefore in this paper we consider both cases.

The efficient operation requires that the dimensions of our device, i.e., the radius of curvature of the convex mirror and the size of the output window, correspond to the available pumping power, spectroscopic properties of the medium, and mirror reflectivities. In Section 2 ray tracing is used to estimate the size of the output window required for efficient coupling of the generated light.

2. RAY TRACING

To predict the properties of a laser with an unstable resonator, we have to estimate the magnification coefficient and the size of the output window. This window should be large enough to allow all the signal rays to get out, but should not be too large because we do not want to pump the region where the signal does not go. Also, we should estimate the parameters of the output signal beam. In this section, we perform these estimates with the ray tracing method.

A. Size of the Output Window

The aspect ratio of the width of the resonator to the length is large, so the Fresnel numbers are large, of the order of 10^6 for the cases considered below. Therefore geometrical optics is applicable. Assuming that the seed region is small, we consider only the axial rays; we let them be in the x,y plane. We let the equation of the plane mirror be $y=0$ and that of the spherical mirror be $x^2+(y-h-r_0)^2=r^2$, as shown in Fig. 3.

We consider rays that originate close to the optical axis. To simplify the ray tracing, we consider the image of a spherical mirror in the plane mirror. Then our resonator becomes equivalent to the symmetrical resonator considered by Siegman,[15] p. 875, example 22(a).

At the ith round trip, the ray comes to point (X_i, Y_i) at the spherical mirror (or its image, as shown in Fig. 3) with an angle β_i. The mirror at this point is inclined with angle $\gamma_i=\arcsin(X_i/r_0)$. After reflection, the angle of inclination of the ray becomes

$$\beta_{i+1}=\beta_i+2\arcsin(X_i/r_0). \tag{1}$$

This ray reaches the spherical mirror again at a point with coordinates (X_{i+1}, Y_{i+1}) such that

$$X_{i+1}-X_i=t_i(|Y_i|-|Y_{i+1}|), \tag{2}$$

$$X_{i+1}^2+(|Y_{i+1}|-h-r_0)^2=r_0^2, \tag{3}$$

where

$$t_i=\tan(\beta_{i+1}). \tag{4}$$

Then the appropriate solution of Eqs. (2) and (3) can be expressed as follows:

$$|Y_{i+1}|=h+\frac{r-\xi_i-[(r-\xi_i)^2-(1+t_i^2)\xi_i^2]^{1/2}}{1+t_i^2}, \tag{5}$$

$$X_{i+1}=X_i+(|Y_i|+|Y_{i+1}|)t_i, \tag{6}$$

$$\xi_i=(X_i+|Y_i|t_i+ht_i)t_i. \tag{7}$$

This solution is shown in Fig. 3 with thin lines. Then we choose the appropriate i, and, to release all the rays, we put the output window between the traced ray at the ith iteration and the ray at the $(i+1)$th iteration. This defines the radius of the spherical mirror $r_1=X_i$, the resulting thickness of the device $H=|Y_i|\approx h+r_1^2/(2r_0)$, and the radius of the device $r_2=r_1+2t_i|Y_i|$. This shape and the reconstructed rays are shown in Fig. 3 with thick lines. Such a ray analysis gives the size of the output window r_2-r_1

and the divergence of the output beam $(\beta_{i+1}-\beta_i)/2$ and its direction; it is inclined with angle $(\beta_{i+1}+\beta_i)/2$ to the optical axis. As for the divergence of the beam in the horizontal plane, it should coincide with the angle of convergence of the pump beam. However, the seed of generation provides rays in all directions, but only those rays that go through the pump region are not depleted because of magnification. In such a way, the ray tracing gives parameters for the design of the laser with a short cavity and predicts the transversal properties of the output beam.

The angle β_{i+1} has no need to be small, as no paraxial approximation is used above. This angle may be even larger than the angle of total internal reflection; then some output coupler (not shown in Figs. 1–3) with an appropriate refractive index is necessary. (The same output coupler can also be used to equalize the divergence angle or eliminate the possible astigmatism of the output beam.) The input coupler in the bottom right corner of the device (Fig. 3) is not essential, but it allows us to avoid losses of the pump in the region without a signal.

Variation of the number i of iterations or initial deviation of the ray from the optical axis allows us to obtain various configurations of wide, short lasers with an unstable cavity. The ratio r_2/r_1 should be interpreted as the magnification at the last trip. This ratio is plotted in Fig. 4 as a function of the ratio r_1/r_0 for various values of the ratio h/r_0. These graphics can be used to determine the size r_2 of the device with given properties at the seed region.

The radius r_2 of the laser is limited by the amplification of spontaneous emission and parasitic oscillation. With high reflectivity of mirrors, the gain G can be relatively small, e.g., $Gh \approx 0.1$. Therefore, at moderated values of product Gr_2, the radius r_2 can be much larger than length h; so, from the point of view of manufacturing, such a laser is a thin disk.

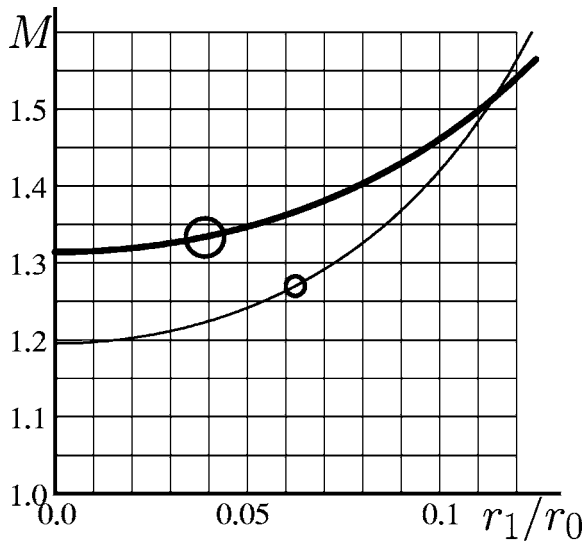

Fig. 4. Magnification $M=r_2/r_1=M(r_1/r_0)$ as a function of the relative size r_1/r_0 of a spherical mirror for $h/r_0=0.039$ [$M(0)=1.196$, thin curve] and $h/r_0=0.002$ [$M(0)=1.314$, thick curve] as a result of ray tracing. The parameters suggested in the text for lasers with Nd and those with Yb are shown with a large and small circle, respectively.

The appropriate technology for the manufacturing of such a device can be the following. First, the flat surface of the disk is polished and will be the bottom flat mirror. After the appropriate coating, the disk is glued to the heat sink, and the upper surface is polished to curvature $1/r_0$. After measuring the resulting thickness h, the appropriate radius r_1 of the mirror is chosen, and the specimen is polished to plane with thickness

$$H = r_0 - (r_0^2 - r_1^2)^{1/2} + h \approx h + r_1^2/(2r_0). \tag{8}$$

This thickness has no need to be precisely adjusted, but the resulting radius r_1 of the mirror should be measured and the required r_2 should be evaluated with the results of this section. Finally, the input window for the pump should be polished and the optional input and output couplers (required in the strongly nonparaxial case) should be glued.

An alternative technology may imply gluing the output window directly on the spherical mirror. This modification increases the amount of material that needs to be polished out, but skips the polishing of the output mirror. Also, at this modification, the edge of the spherical mirror can be semitransparent, avoiding diffraction of the output signal at this edge and improving the beam quality of the output signal. The physics of such a modified device is the same; so, in the following, we refer to the initial scheme shown in Figs. 1–3.

Although the paraxial approximation is not used in this section to determine the dimensions of the device, we use this approximation in this paper to estimate the efficiency of the device. In the paraxial case, the magnification does not depend on the radius r_1 of the mirror, and the formulas above can be simplified. This case is considered in Ref. 15, p. 875, table 22.1a. In our notations, the magnification coefficient is

$$M = \frac{X_{i+1}}{X_i} = 1 + 2\left[\frac{h}{r_0}\left(1 + \frac{h}{r_0}\right)\right]^{1/2} + 2\frac{h}{r_0}. \tag{9}$$

Equation (9) can also be obtained by asymptotic analysis of Eqs. (1)–(7). It corresponds to the left-hand side of the graphics in Fig. 4. In this approximation, all the output originates from the same virtual point $\{0, -[h(h+r_0)]^{1/2}\}$. This point is called the virtual source; the size of the output window determines the NA of the output signal. In such a way, the spatial properties of the output beam are determined by the geometry of the device. The basic formulas of this section and examples of values are given in the bottom half of Table 3.

B. Seed Region and Beam Quality of Pump

To describe the properties of the suggested laser, we need to estimate the size of the seed region. Then we use this estimate to formulate the criteria for the properties of the pump beam, NA, and the beam quality, which allow almost uniform illumination of the region required.

For scaling to the high power, the noncoherent combining of several pump beams makes the divergence of the pump beam much stronger than the diffractional limit. The geometry of a scalable laser should take into account this property. For the laser shown in Fig. 2, we do not need to pump the whole domain; only one sector of the

disk should be pumped. Then the pump should be focused into the optical axis. This focusing can partially compensate the depletion of power of the pump; then the active medium will work in the most efficient regime, providing good performance of the device.

The size of the seed of the laser oscillation at the optical axis can be estimated using the concept of the equivalent Fresnel number (see Ref. 15, p. 872). Consider a similar cavity with small mirror of size w. In our case, the equivalent Fresnel number can be expressed as

$$N_{\mathrm{eq}} = \frac{nw^2}{2h\lambda_{\mathrm{s}}}\left(M - \frac{1}{M}\right), \tag{10}$$

where n is the refractive index, h is the length of the resonator (or half-length if we consider the equivalent expanded symmetric resonator, as shown in Fig. 3), and M is the magnification coefficient considered in Subsection 2.A. This N_{eq} measures the optical length difference, in units of λ_s, between the edge of the mirror and the wave front that touches the mirror at the optical axis. This parameter is crucial for the behavior of unstable cavities, as it determines losses $\mathcal{L}$ of the principal mode. At high values of $N_{\mathrm{eq}} \gg 1$, the losses are determined by the magnification coefficient M and the reflectivity R of the mirrors; $1-\mathcal{L}=R^2/M^2$. (We assume that both mirrors have equal reflectivity.) As we reduce N_{eq}, the losses show oscillations, but at $N_{\mathrm{eq}}<1$ the losses $\mathcal{L}$ increase and the quality of the resonator quickly decays. To avoid strong losses, the pump should illuminate the first equivalent Fresnel zone, which would correspond to $N_{\mathrm{eq}}=1$. This gives an estimate of the waist of the pump at the optical axis:

$$w = \left(\frac{2h\lambda_s/n}{M - 1/M}\right)^{1/2}. \tag{11}$$

There is no reason to focus the pump beam to the strip much narrower than this w because the losses of the signal mode due to the cutting at the edges of the gain will greatly offset the increase of gain due to the strong pump focusing. Therefore this w can be interpreted as the waist of the pump beam in the horizontal direction.

In the case of a pump ray with diffractional quality, this would correspond to the pump beam with a convergence angle λ_p/nw. However, at the combining of m pump beams in a row, the angle would be at least $q^{-1}=m/2$ times larger. The pump is supposed to be confined in the vertical direction; the factor 2 appears in the denominator because of the possibility to combine beams with both polarizations. The parameter q can be interpreted as the beam quality of the pump. (Sometimes the notation M factor is used instead of $1/q$, but we use the notation q to avoid confusion with magnification M of the resonator.) Then the angle

$$\mathrm{NA} = \frac{\lambda_p}{nqw} \tag{12}$$

should be interpreted as the NA of the pump beam inside the medium. The NA of the incident beam can be recalculated from this NA, taking into account the shape of the input window (it can be a plane and it can be cylindrical as shown in Fig. 1).

As is mentioned in Refs. 12 and 13, the medium works especially efficiently if the depletion of the pump is compensated with its concentration in such a way that the pump intensity remains approximately constant. Let us formulate the conditions of an approximately constant intensity for our case. The spot size $w(z)$ of the Gaussian beam can be expressed as follows:

$$w(z) = w_0\left[1 + \left(\frac{\lambda z}{\pi q w_0^2}\right)^2\right]^{1/2}, \tag{13}$$

where $w_0=2\lambda_p/q\pi\mathrm{NA}$ is the waist of the pump beam. (For a diffraction-limited pump, we would have $q=1$ and the waist w would be the same as in the case of a coherent Gaussian beam.[15]) In the absence of absorption, the intensity versus length z of propagation would behave as $1/w(z)$. The pump is confined between two mirrors, so we neglect the dependence of the pump intensity along the optical axis of the resonator. Only diffraction in the plane of the mirror takes place. Then the reduction of w may partially compensate depletion of power in such a way that the intensity remains almost constant. However, the function $1/w(z)$ cannot completely compensate the exponential decay of the pump power because of absorption, but the approximate compensation takes place at

$$\exp(-Ar_2) = \frac{w}{\mathrm{NA}\, r_2}, \tag{14}$$

where A is the saturated absorption of the pump. We assume that the beam quality of the pump

$$q = \frac{\lambda_p}{2nw\ \mathrm{NA}} \tag{15}$$

allows its focusing onto a strip of width $2w$ at the optical axis of the cavity. The distribution of intensity of the pump in the plane orthogonal to the optical axis of the resonator can be approximated as follows:

$$\frac{I_p(x_1,x_2)}{I_p(0,r_2)} \approx u(x_1)\exp\left[-\left(\frac{x_2}{w(x_1)}\right)^2\right],$$

$$u(r) = \frac{r_2\exp(Ar)}{\{r_2^2 + [\exp(2Ar_2)-1]r^2\}^{1/2}}. \tag{16}$$

Function $u(r)$ by approximation (16) is plotted in Fig. 5(b). At positive values of r, this parameter can be interpreted as a radial coordinate of the cylindrical system centered at the optical axis of the resonator. For comparison, in Fig. 5(b) we plot the exponential profile with the same decrement A, which would take place if the pump was not focused. Two vertical lines at $r=\pm 0.04$ mm mark the typical size of the seed area of the resonator shown in Figs. 1–3. For a $\eta_p=80\%$ absorption efficiency, the variation of intensity does not exceed 15%.

C. Properties of the Signal Beam

We expect the output to be a single transverse mode. We suggest a short speculation in favor of this expectation. In the seed region, the field of the signal is paraxial, and the scaling transformation of a mode Ψ at the round trip can be written as follows:

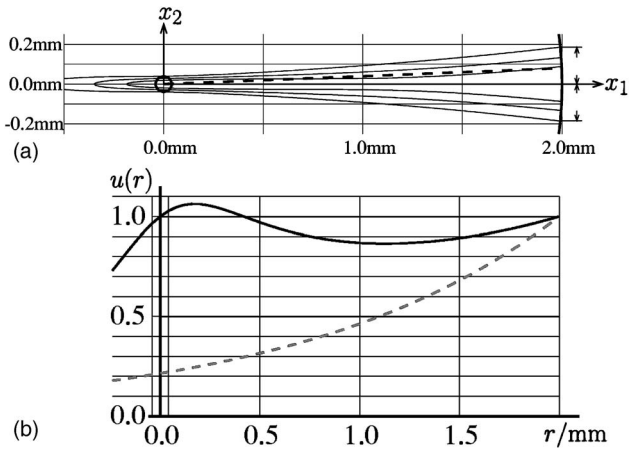

Fig. 5. Example of distribution of intensity in the vicinity of the pump beam, calculated by approximation (16). (a) Contour lines of pump intensity focused from radius $r_2=2$ mm with a NA of 0.091 into the seed region (shown by the circle) or radius $w=0.04$ mm; levels $\exp(-1)$, 0.6, 0.8 are marked. (b) Distribution of intensity along the direction of propagation of the pump. The solid curve is the profile of intensity $u(r)$ for $r_2=2$ mm, $A=0.769$/mm. The dashed curve is the exponential profile $\exp[-A(r_2-r)]$.

$$\Psi(x) \to \frac{R\exp(Gh)}{M}\Psi\left(\frac{x}{M}\right), \tag{17}$$

where $x=\{x_1,x_2\}$ and x_1, x_2 are transversal coordinates.

The principal mode gets magnified with coefficient M, which reduces its intensity M^2 times. This reduction, together with losses at the mirror, is compensated by the gain. The principal mode of the resonator is almost flat in the vicinity of the optical axis, $\Psi \approx$ constant. The transformation of relation (17) should be identical for the principal mode as this determines the saturated gain G in terms of the parameters of the resonator.

In the seed region, the first excited mode is approximately proportional to some coordinate $\tilde{x}$, which is a linear combination of x_1 and x_2 shown in Fig. 5(a). Such a mode can be written as

$$\Psi_1(x) = \tilde{x}\psi_f(x), \tag{18}$$

where $\psi_f(x)$ is a smooth function. The substitution of Eq. (18) into relation (17) yields

$$\tilde{x}\psi_f(x) \to \frac{R\exp(Gh)}{M}\frac{\tilde{x}}{M}\psi_f\left(\frac{x}{M}\right). \tag{19}$$

We can see that the amplitude of mode Ψ_1 gets an additional factor $1/M$ at each round trip. At values of the magnification coefficient $M \approx 1.2$, we have good conditions for discrimination of higher transverse modes.

Consider now the behavior of the principal mode outside of the region of the seed of generation. This region is marked with a circle in Fig. 5(a). Outside of the seed region, we can use geometrical optics. The projection of one ray of a signal originating at the seed region is shown with a dashed line. This ray feels almost constant pump intensity. The significant difference in intensity appears only for rays that are well out from the aperture of the pump beam; they quickly leave the pumped region. This justifies our statement that most of the signal should be emitted in the direction of the pump (see Figs. 1 and 2) with the same aperture.

Each ray of signal, originating in the seed region, feels some pump intensity almost constant along its propagation in the medium. The different rays of signal may have different intensities, but the same phase, as they come from the diffraction-limited spot. The difference in intensities does not cause the diffraction because of huge Fresnel numbers. Therefore we can consider each ray independently in the approximation of constant intensity.

To estimate the properties of the output signal, we use the paraxial approximation. In this approximation, all the rays of the signal come from the same virtual point at the optical axis of the resonator. This point is localized at distance

$$Z_0 = [(r_0 + h)h]^{1/2} \tag{20}$$

from the plane mirror. While $h \ll r_0$, we can estimate the NA of the output signal beam

$$\mathrm{NA}_1 = (r_2 - r_1)/(2Z), \quad \mathrm{NA}_2 = \mathrm{NA}_p/(Z) \tag{21}$$

in two directions, where $Z=Z_0/n$ and n is the index of refraction. In general, the output signal beam may have astigmatism, so we specify two values of the NA.

The output of the signal is expected to be single mode. In the paraxial approximation, such a laser should also provide good beam quality at the output. As mentioned in Section 1, the laser has no need to work in the paraxial regime. The output of such a nonparaxial device may be single mode, but the beam quality may be nonideal. However, it can be corrected with a passive output coupler. The single-mode output of a nonparaxial laser can be converted to high beam quality by using a passive element.[16] The analysis of such a correction is outside the scope of this paper.

In this paper we estimate mainly the slope efficiency of the proposed laser. This slope efficiency is the same for all rays within the aperture of the pump. Being well pumped, such a laser provides a signal with an intensity profile that follows the profile of the pump, and the projection of the virtual point is the center of the seed region. Therefore, to estimate the slope efficiency, we have no need to consider many rays. We may estimate the slope efficiency for the central ray [its projection coincides with axis x_1 in Fig. 5(a)] and extrapolate the estimate to the whole device. In this approximation, the saturated gain is determined by the magnification of the resonator and the reflection coefficient R of the mirrors.

Assuming the uniform distribution of intensities along the ray of the signal, we conclude that

$$\frac{R^2}{M^2}\exp(2Gh) = 1, \tag{22}$$

where G is the saturated gain and R is the reflection coefficient; we assume that this coefficient is the same at both mirrors of the resonator. However, we need some model of the gain medium to estimate the intensity of the signal at which the gain G satisfies Eq. (22).

3. MODEL OF THE MEDIUM

In this section we analyze the simple model with two manifolds of levels. We apply this model to the case of Nd:YAG and Yb:YAG ceramics. This approximation seems to work well not only for Nd:YAG[4,8,9] and Yb:YAG[2] but also for media made of different host–dopant combinations (e.g., Nd:YVO_4 or Er:silica at moderated concentrations[17]) can be described with the same equations below.

A. Local Rate Equations

Assume that the medium has two manifolds of levels such that all the relaxation processes within each manifold are fast in comparison to the rates of transition between these two manifolds. Let N be the concentration of active centers, τ be radiative lifetime of the upper laser manifold, and $\sigma_a(\lambda)$ and $\sigma_e(\lambda)$ be the effective cross sections of absorption and emission at wavelength λ.

Let n_1 and n_2 be the relative populations at the lower and upper manifolds, $n_1=N_1/N$, $n_2=N_2/N$. Then $n_1+n_2=1$. The kinetic equations for these populations can be written as follows:

$$\partial n_2/\partial t = -W_u n_1 + W_d n_2, \tag{23}$$

$$\partial n_1/\partial t = W_u n_1 - W_d n_2, \tag{24}$$

where

$$W_u = \frac{I_p \sigma_{\mathrm{ap}}}{\hbar\omega_p} + \frac{I_s \sigma_{\mathrm{as}}}{\hbar\omega_s}, \quad W_d = \frac{I_p \sigma_{\mathrm{ep}}}{\hbar\omega_p} + \frac{I_s \sigma_{\mathrm{es}}}{\hbar\omega_s} + \frac{1}{\tau} \tag{25}$$

are the transition rates for the absorption and relaxation. Here I_p and I_s are local intensities of pump and signal; σ_{ap} and σ_{ep} are effective absorption and emission cross sections at frequency ω_p of pump; and σ_{as} and σ_{es} are the same for the signal frequency ω_s. The steady-state solution for n_1 and n_2 can be written as follows:

$$n_1 = \frac{W_d}{W_u + W_d}, \quad n_2 = \frac{W_u}{W_u + W_d}. \tag{26}$$

Let the medium be pumped at wavelength λ_p, and let it lase at wavelength λ_s, so $\omega_p=2\pi c/\lambda_p$, $\omega_s=2\pi c/\lambda_s$, where c is the speed of light. The dynamic saturation intensities can be defined as follows:

$$I_{\mathrm{po}} = \frac{\hbar\omega_p}{(\sigma_{\mathrm{ap}} + \sigma_{\mathrm{ep}})\tau}, \quad I_{\mathrm{so}} = \frac{\hbar\omega_s}{(\sigma_{\mathrm{as}} + \sigma_{\mathrm{es}})\tau}. \tag{27}$$

We define the absorption at strong signal A_0 and gain at strong pump G_0 as follows:

$$A_0 = \frac{N\mathcal{D}}{\sigma_{\mathrm{as}} + \sigma_{\mathrm{es}}}, \quad G_0 = \frac{N\mathcal{D}}{\sigma_{\mathrm{ep}} + \sigma_{\mathrm{ap}}}, \tag{28}$$

where

$$\mathcal{D} = \sigma_{\mathrm{ap}}\sigma_{\mathrm{es}} - \sigma_{\mathrm{ep}}\sigma_{\mathrm{as}}. \tag{29}$$

Then the local absorption of pump $A=N(n_2\sigma_{\mathrm{ap}}-n_1\sigma_{\mathrm{ep}})$, local gain $G=N(n_2\sigma_{\mathrm{es}}-n_1\sigma_{\mathrm{as}})$, and local quantum efficiency η_q and local efficiency of medium η_m can be expressed as follows:

$$A = A_0\frac{U+s}{1+p+s}, \quad G = G_0\frac{p-V}{1+p+s}, \tag{30}$$

$$\eta_q = \frac{1-V/p}{1+U/s}, \quad \eta_m = \frac{I_s G}{I_p A} = \frac{\lambda_p}{\lambda_s}\eta_q, \tag{31}$$

where $p=I_p/I_{po}$, $s=I_s/I_{so}$, $U=(\sigma_{\mathrm{as}}+\sigma_{\mathrm{es}})\sigma_{\mathrm{ap}}/\mathcal{D}$, $V=(\sigma_{\mathrm{ap}}+\sigma_{\mathrm{ep}})\sigma_{\mathrm{as}}/\mathcal{D}$. As $U-V=1$, Eqs. (30) lead to the following identity:

$$\frac{A}{A_0} + \frac{G}{G_0} = 1, \tag{32}$$

which simplifies the analysis.

In the steady-state cw generation, the gain compensates the losses; and Eq. (22) determines the gain G. Then Eq. (32) defines the absorption A. Also, we can express the corresponding intensity of the signal as a function of the intensity I_p of the pump using the second Eq. (30). This will lead to the estimate of the efficiency of the laser. The appropriate weighting of the local efficiency of the medium by Eqs. (31) can be used to deduce an independent estimate of the efficiency of the laser.

B. Nd:YAG and Yb:YAG

The properties of the medium depend mainly on the emission and absorption cross sections of the working transitions. For the ceramics available, the absorption and emission rates were measured; the resulting spectra of emission and absorption are shown in Fig. 6.

One objective is to provide simple estimates of quantities relevant to the design of such a laser. Therefore we fit the cross sections with elementary functions. For Nd:YAG we use

$$\sigma_a(\lambda) \approx f_0(\lambda/\mathrm{nm}) \times 10^{-20}\ \mathrm{cm}^2, \tag{33}$$

$$\sigma_e(\lambda) \approx f_1(\lambda/\mathrm{nm}) \times 10^{-20}\ \mathrm{cm}^2, \tag{34}$$

where

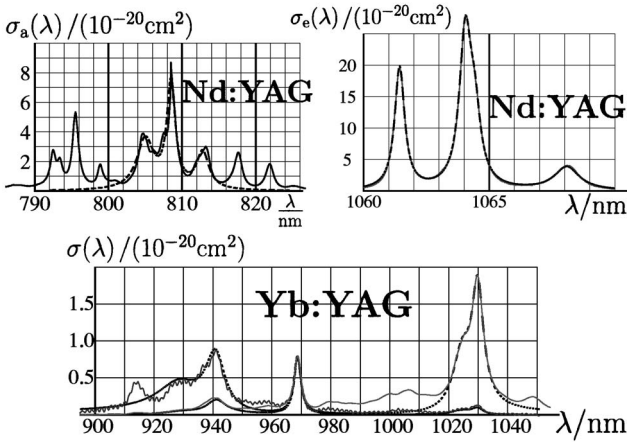

Fig. 6. Affective absorption and emission cross sections for Nd:YAG and Yb:YAG (solid curves); fits of approximations (33) and (34) for Nd and approximations (36) and (37) for Yb (dashed curves).

Table 1. Parameters of the Fits of Eqs. (33)–(35)

j	K_j	m	$a_{j,m}$	$b_{j,m}$	$c_{j,m}$
0	3	1	3.4	805.0	1.4
		2	7.1	808.5	0.7
		3	2.5	812.8	1.0
1	4	1	19.4	1061.431	0.24
		2	23.9	1064.047	0.29
		3	9.9	1064.42	0.28
		4	3.7	1068.09	0.6

Table 2. Parameters of the Fit of Eq. (38)

m	a_m	b_m	c_m
1	0.13	929.0	8.5
2	0.38	941.0	4.0
3	0.78	968.7	1.4
4	0.21	1024.5	4.0
5	0.36	1029.8	2.3

$$f_j(x)=\sum_{m=1}^{K_j}\frac{a_{j,m}}{1+\left(\frac{x-b_{j,m}}{c_{j,m}}\right)^2},\quad j\in\{0,1\}. \tag{35}$$

The parameters of these fits are given in Table 1.

For Yb:YAG, the McCumber theory (see Ref. 17, pp. 104–105) allows one to approximate two functions with the same fit:

$$\sigma_a(\lambda)\approx f_3(\lambda/\mathrm{nm})\exp(\Lambda/\lambda-\Lambda/\lambda_0)\times 10^{-20}\ \mathrm{cm}^2, \tag{36}$$

$$\sigma_e(\lambda)\approx f_3(\lambda/\mathrm{nm})\exp(\Lambda/\lambda_0-\Lambda/\lambda)\times 10^{-20}\ \mathrm{cm}^2, \tag{37}$$

$$f_3(x)=\sum_{m=1}^{5}\frac{a_m}{1+\left(\frac{1/x-1/b_m}{c_m/b_m^2}\right)^2}, \tag{38}$$

where $\Lambda=\pi\hbar c/K_BT$; $\lambda_0=964.6$ nm; $T=300$ K is the temperature; K_B is the Boltzmann constant; and parameters a_m, b_m, c_m are found in Table 2. These fits are shown in Fig. 6 with dashed curves. They satisfactorily reproduce cross sections around the pump and signal wavelengths. These fits will be used for the analysis of the efficiency and stability of the SLM generation.

C. Spatial Hole Burning

The interaction of coherent waves inside a laser causes SHB. This effect slightly reduces the efficiency of standing-wave lasers and may cause instabilities of the single-mode generation. The weak signal with a slightly different wave vector may have an advantage, as the maxima of its intensity are not correlated with the minima of gain. Here we analyze the conditions of the SLM generation.

Let I_1 and I_2 be the intensities of counterpropagating waves of the signal and $s_1=I_1/I_{so}$ $s_2=I_2/I_{so}$ be the corresponding normalized intensities. The efficient diffusion of excitations in the active medium discussed in Ref. 18, or the forced displacement of the interference picture used in Ref. 10, as well as orthogonal polarization of the counterpropagating waves (twisted modes),[9] eliminate the grating produced by the counterpropagating waves. In this case, no SHB takes place; the medium feels only the sum of the intensities, the effective gain is the same for both waves, and Eqs. (30) and (31) can be used with the substitution of $s=s_1+s_2$.

In the case when the response of the medium is local and when the counterpropagating waves have the same polarization, the formulas above overestimate the gain, local absorption rate, and efficiency. This case is analyzed in Refs. 5, 6, and 18. For our model, this analysis gives the following expressions for the absorption rate A, the gain of the first wave G_1, and the quantum efficiency of the medium:

$$A=A_0\frac{1}{\pi}\int_0^{\pi}\frac{U+s_1+s_2+2\sqrt{s_1s_2}\cos(\theta)}{1+p+s_1+s_2+2\sqrt{s_1s_2}\cos(\theta)}\mathrm{d}\theta$$
$$=A_0\left\{1-\frac{1+p-U}{[(1+p+s_1+s_2)^2-4s_1s_2]^{1/2}}\right\}, \tag{39}$$

$$G_1=G_0\frac{1}{\pi}\int_0^{\pi}\frac{1+\sqrt{s_2/s_1}\cos(\theta)}{1+p+s_1+s_2+2\sqrt{s_1s_2}\cos(\theta)}\mathrm{d}\theta$$
$$=G_0\frac{p-V}{2s_1}\left\{1-\frac{1+p+s_2-s_1}{[(1+p+s_1+s_2)^2-4s_1s_2]^{1/2}}\right\}, \tag{40}$$

$$\eta_q=\frac{1-V/p}{1+\frac{U}{[(1+p)^2+2(1+p)(s_1+s_2)+(s_1-s_2)^2]^{1/2}-1-p}}. \tag{41}$$

The effective gain of the second wave can be obtained from Eq. (40) by substituting the subscripts 1 and 2. Note that at $s_2=0$, Eqs. (39)–(41) are equivalent to Eqs. (30) and (31), and Eq. (32) becomes valid again.

The uncorrelated field at wavelength λ feels the mean gain

$$\tilde{G}=\tilde{G}(\lambda)=\frac{N}{\pi}\int_0^{\pi}[n_2\sigma_e(\lambda)-n_1\sigma_a(\lambda)]\mathrm{d}\theta, \tag{42}$$

where the populations n_1 and n_2 are evaluated by Eqs. (25)–(27) in substitution $I_p=I_{po}p$, $I_s=I_{so}s$ for the normalized pump intensity p and the normalized signal intensity $s=s_1+s_2+2\sqrt{s_1s_2}\cos\theta$. Performing the integration, we obtain

$$\tilde{G}(\lambda)=\frac{1}{b}\left[d+\frac{bc-ad}{(a^2-b^2)^{1/2}}\right],$$

$$\text{where}\begin{cases} a = 1 + p + s_1 + s_2 \\ b = 2\sigma_1\sqrt{s_1 s_2} \\ c = \sigma_2 p - \sigma_a + \sigma_1(s_1 + s_1) \\ d = \sigma_1(s_1 + s_2) \\ \sigma_1 = \dfrac{\sigma_{as}\sigma_e - \sigma_{es}\sigma_a}{\sigma_{as} + \sigma_{es}} \\ \sigma_2 = \dfrac{\sigma_{ap}\sigma_e - \sigma_{ep}\sigma_a}{\sigma_{ap} + \sigma_{ep}} \\ \sigma_a = \sigma_a(\lambda);\ \sigma_e = \sigma_e(\lambda) \end{cases}. \tag{43}$$

This expression is used in Section 4 for the stability analysis of the single-mode oscillation.

In the case $s_1 = s_2$, we substitute each of these two intensities to $s/2$. Then

$$A = A_0\left\{1 - \frac{1 + p - U}{[(1+p)^2 + 2(1+p)s]^{1/2}}\right\}, \tag{44}$$

$$G_1 = G_0\frac{p - V}{s}\left\{1 - \frac{1 + p}{[(1+p)^2 + 2(1+p)s]^{1/2}}\right\}, \tag{45}$$

$$\eta_q = \frac{1 - V/p}{1 + \dfrac{U}{[(1+p)^2 + 2(1+p)s]^{1/2} - 1 - p}}. \tag{46}$$

Equation (46) shows that, for the efficient operation of a medium with SHB, it is not sufficient that $p \gg V$ and $s \gg U$ (as in the case without SHB); we should also have $U/(p+1)/[1+2s/(1+p)]^{1/2} - 1 \ll 1$.

For small values of s, Eq. (45) is not very good; we suggest

$$G_1 = G_0\frac{2(p - V)}{1 + p + 2s + [(1+p)(1+p+2s)]^{1/2}}. \tag{47}$$

The deduction of Eq. (47) from Eq. (45) could be a good exercise for students. The representation in Eq. (47) is used in Section 5 to extract the normalized intensity s of the signal as a function of G and p.

We collect the notations and basic formulas of this section in the first part of Table 3 and suggest two examples of values of the parameters for Nd:YAG and Yb:YAG. These formulas together with the fits of Eqs. (33)–(38) describe the behavior of the medium in terms of elementary functions, and this description is not specific for our laser configuration.

4. MODEL OF THE LASER

In this section we combine the results of Sections 2 and 3 to describe the laser. First we neglect the SHB. Then we show that SHB has a minimal change on the estimate of the efficiency. Then we analyze conditions of the single-mode operation.

A. Laser without Spatial Hole Burning

Assume that the medium feels the total intensity of the signal as the sum of intensities of the wave going forward and the wave going backward. In the steady-state cw regime, the gain is determined by the properties of the resonator. From Eq. (22), we obtain

$$G = \frac{\ln(M/R)}{h}. \tag{48}$$

Equations (48) and (32) allow us to express the local absorption rate as

$$A = A_0\left[1 - \frac{\ln(M/R)}{G_0 h}\right]. \tag{49}$$

Then we can estimate the absorption efficiency of the pump:

$$\eta_p = 1 - \exp(-Ar_2). \tag{50}$$

This gives an estimate for the reasonable size of the device. To provide efficient absorption of the pump in the gain medium, the radius r_2 of the device should be of the order of $1/A$ or greater.

To estimate the resulting efficiency of the laser, we need to express the intensity of the signal in terms of gain and the pump intensity. Solving the second Eq. (30) with respect to s, we obtain

$$s = \left(\frac{G_0}{G} - 1\right)p - \frac{G_0}{G}V - 1 = \delta_i(p - p_t), \tag{51}$$

where the coefficient $\delta_i = \mathrm{d}s/\mathrm{d}p$ can be interpreted as some normalized slope of intensity (this slope has no need to be smaller than unity), and $p_t = [(G_0/G)V + 1]/\delta_i$ is the normalized threshold pump intensity.

While we know the relative sizes of the input and output windows and relations $I_s = sI_{so}$ and $I_p = sI_{po}$ between the normalized intensities and the intensities, we can express the power of the pump in terms of the normalized pump intensity and the same of the signal:

$$P_p = 2L(r_2 - r_1)I_{so}p, \tag{52}$$

$$P_s = L(r_2 - r_1)I_{so}s. \tag{53}$$

These formulas take into account the fact that only half of the signal intensity goes to the mirror with an output window (up in Figs. 1–3, whereas the whole pump power goes through the input window.

Combining Eqs. (51)–(53), we express the output signal power in terms of input pump power:

$$P_s = \eta_{\text{slope}}(P_p - P_{\text{th}}), \tag{54}$$

where

$$P_{\text{th}} = 2LhI_{po}p_t \tag{55}$$

should be interpreted as the threshold pump power, and

$$\eta_{\text{slope}} = \left(\frac{G_0}{G} - 1\right)\frac{I_{so}}{I_{po}}\frac{r_2 - r_1}{2h} \tag{56}$$

should be interpreted as the slope efficiency. In Eq. (56) the output power is a linear function of the input power.

Let us analyze the error of our estimate. The actual intensity of the pump varies according to the profile shown in Fig. 5; let u_- and u_+ be the minimal and maximal val-

Table 3. General Properties of Media and Examples of Resonators

Quantity	Expression	Example Nd:YAG	Example Yb:YAG
Lifetime	τ	0.25×10^{-3} s	0.97×10^{-3} s
Atomic concentration	N_{at}	1%	10%
Concentration	N	1.380×10^{26} m^{-3}	26.660×10^{26} m^{-3}
Index of refraction	n	1.820	1.820
Pump wavelength	λ_p	808.5 nm	940.0 nm
Signal wavelength	λ_s	1064.2 nm	1029.6 nm
Pump absorption cross section	$\sigma_{ap}=\sigma_a(\lambda_p)$	7.6972×10^{-20} cm^2	0.8738×10^{-20} cm^2
Pump emission cross section	$\sigma_{ep}=\sigma_e(\lambda_p)$	0.0001×10^{-20} cm^2	0.1917×10^{-20} cm^2
Signal absorption cross section	$\sigma_{as}=\sigma_a(\lambda_s)$	0.0002×10^{-20} cm^2	0.1021×10^{-20} cm^2
Signal emission cross section	$\sigma_{es}=\sigma_e(\lambda_s)$	26.2989×10^{-20} cm^2	1.8988×10^{-20} cm^2
Pump saturation intensity	$I_{po}=\dfrac{2\pi\hbar c}{\tau\lambda_p(\sigma_{ap}+\sigma_{ep})}$	127.7 W/mm^2	204.5 W/mm^2
Signal saturation intensity	$I_{so}=\dfrac{2\pi\hbar c}{\tau\lambda_s(\sigma_{as}+\sigma_{cs})}$	28.4 W/mm^2	99.4 W/mm^2
Determinant of cross sections	$D=\sigma_{ap}\sigma_{es}-\sigma_{ep}\sigma_{as}$	202.43×10^{-40} cm^4	1.64×10^{-40} cm^4
Maximal pump absorption	$A_{\max}=N\sigma_{ap}$	1.0622 mm^{-1}	2.3295 mm^{-1}
Pump absorption at strong signal	$A_0=ND/(\sigma_{as}+\sigma_{es})$	1.0622 mm^{-1}	2.1846 mm^{-1}
Signal gain at strong pump	$G_0=ND/(\sigma_{ap}+\sigma_{ep})$	3.6292 mm^{-1}	4.1026 mm^{-1}
Normalized displacement of signal	$U=(\sigma_{as}+\sigma_{es})\sigma_{ap}/D$	1.000007	1.066343
Normalized displacement of pump	$V=(\sigma_{ep}+\sigma_{ap})\sigma_{as}/D$	0.000007	0.066343
Medium transparency threshold	$I_{pt}=I_{po}V$	0.0 W/mm^2	13.6 W/mm^2
Signal needed for efficiency	$I_{sf}=I_{so}U$	28.4 W/mm^2	106.0 W/mm^2
Length of resonator	h	0.75 mm	0.16 mm
Radius of device	r_2	2.00 mm	1.50 mm
Radius of curvature	r_0	40 mm	20 mm
Magnification	$M=1+2\left[\dfrac{h}{r_0}\left(1+\frac{h}{r_0}\right)\right]^{1/2}+2\frac{h}{r_0}$	1.314	1.196
Distance to virtual source	$Z=[h(r_0+h)]^{1/2}/n$	3.038 mm	0.987 mm
Size of seed	$w=\left(\dfrac{2\lambda_s h/n}{M-1/M}\right)^{1/2}$	0.040 mm	0.022 mm
Reflection factor of the mirrors	R	0.95	0.95
Saturated gain	$G=\dfrac{\ln(M/R)}{h}$	0.432 mm^{-1}	1.437 mm^{-1}
Efficiency of signal coupling	$\eta_s=\dfrac{M-1}{M-R}$	0.863	0.796
Dimensionless threshold	$p_t=\dfrac{VG_0+G}{G_0-G}$	0.1353	0.6413
Pump intensity threshold	$I_{pr}=p_t I_{po}$	17 W/mm^2	131 W/mm^2
Radius of mirror, paraxial	$r_1=r_2/M$	1.52 mm	1.25 mm
Radius of device, ray tracing	r_2	2.03 mm	1.68 mm
Size of output window, paraxial	r_2-r_1	0.48 mm	0.25 mm
Size of output window, ray tracing	r_2-r_1	0.52 mm	0.33 mm

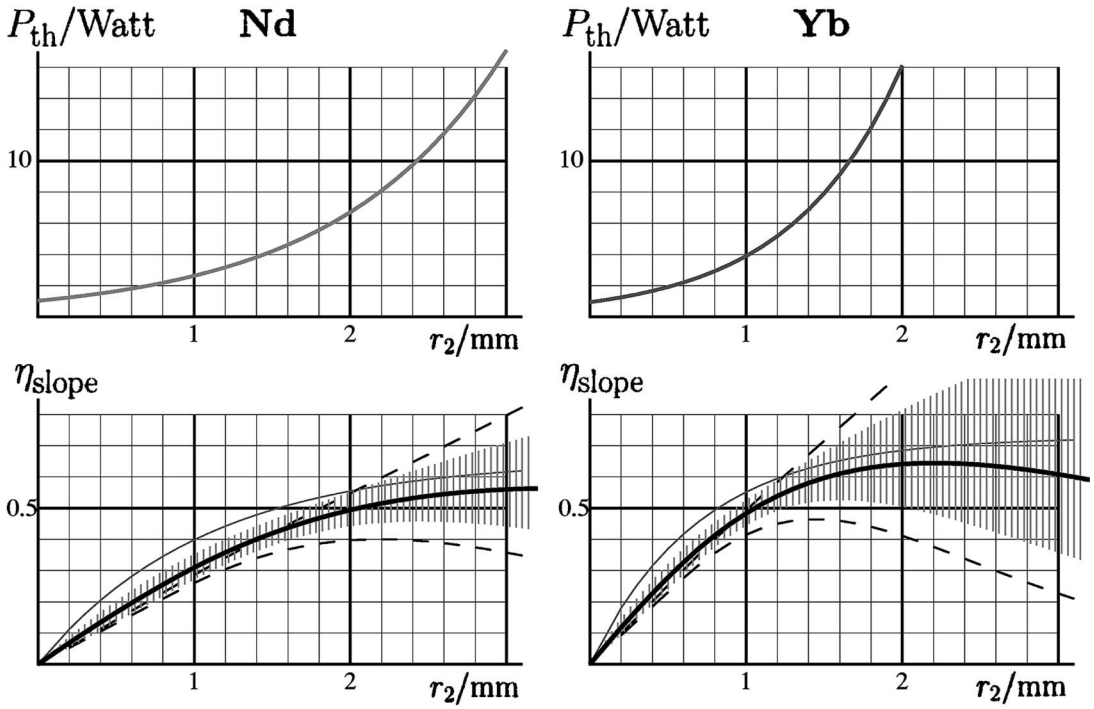

Fig. 7. Upper graphics: Pump threshold power P_{pt} by Eq. (41) for the case with Nd and Yb. Lower graphics: Estimates of the slope efficiency without hole burning. The two dashed curves show the optimistic and pessimistic estimates $\eta_{\pm}=I_{so}/I_{po}[(G_0/G)-1](r_2-r_1/2h)u_{\pm}$. The thin solid curves show independent estimate $\eta_3=(\lambda_s/\lambda_p)\eta_p\eta_s$. The thick curves show the mean geometric values of three estimates above; the corresponding error bars are cut at $\eta=\lambda_p/\lambda_s$.

ues of the intensity profile shown. Applying these coefficients to the estimate above, we obtain both the optimistic and the pessimistic estimates of the slope efficiency $\eta_{\pm}=\eta_{\text{slope}}u_{\pm}$. These estimates are shown in Fig. 7 with dashed curves; they can already be used for the predictions of the properties of such a device.

The optimistic estimate shows almost linear growth at large values of r_2; the pessimistic one shows almost exponential decay, and some reasonable average between them could give a reasonable fit of experimental data. As we still lack such data, the heuristic weighted estimate could be useful. Such a heuristic estimate can be obtained on the basis of the law of conservation of energy.

In the estimates above, we were tracing the power as it transfers from pump light at the input window to the medium, then to the signal light inside the cavity, and then to the output window. We can also trace the losses of energy. Not all the pump light is absorbed by the medium before the seed region. The medium does not convert all the power to the signal. Not all the signal power reaches the output window. We already have estimated the efficiency η_m of the medium; in our approximation, the slope efficiency of the medium is just the quantum defect coefficient λ_p/λ_s. We have also estimated the absorption efficiency η_p of the pump [see Eq. (50)]. Hence, we should estimate the efficiency η_s of the output coupling of the signal. The product of these three estimates is an additional (and, in some sense, independent) estimate of the efficiency of the device.

To estimate η_s, note that the output power is proportional to the area of the window $(r_2^2-r_1^2)$ NA. The absorbed power is proportional to the product of the area of mirrors illuminated and the loss coefficient $(1-R)$. The area of mirrors exposed to the signal is r_1^2 NA for the upper window and $0.25(r_1+r_2)^2$ NA for the lower window. The ratio of output power to the sum of output power and absorbed power gives the estimate of the efficiency of the output coupling:

$$\eta_s=\frac{(r_2^2-r_1^2)}{(r_2^2-r_1^2)+r_1^2(1-R)+\left(\frac{r_2+r_1}{2}\right)^2(1-R)}=\frac{M-1}{M-R+\mathcal{O}}, \tag{57}$$

where $\mathcal{O}=(R-1)(M-1)^2/[4(M+1)]$ is small; in the typical case, it is smaller than 10^{-3}, so we replace it by zero. (Relation $r_2=Mr_1$ was used.)

The estimate $\eta_3=\eta_p\eta_m\eta_s$ is shown in the lower part of Fig. 7 with thin solid curves. This estimate shows the portion of total power that goes to the signal. The overlap of the signal with the pump is not complete, especially at small values of r_2, so not all the signal goes to the NA of the pump. For this reason, at small values of r_2 the curve for η_3 is higher than both optimistic and pessimistic estimates that count only the signal that goes to the same NA through which the pump goes through.

The sources of error of the estimates η_+, η_- are different from those of the estimate η_3. Therefore we can treat estimates η_-, η_+, η_3 as if they were independent experimental data and calculate some mean value and plot the error bars. The mean geometric value $\eta_4=(\eta_+\eta_-\eta_3)^{1/3}$ is shown in the lower part of Fig. 7 with thick solid curves. The error bars correspond to the mean-square deviation of the logarithm of the estimate. These error bars indicate the shadowed confidence interval in lower parts of Fig. 7.

In the case of Yb, these error bars exceed the quantum limit, so the upper part of the error bars was truncated.

In Eq. (57) we ignored the fact that, in the region close to the output window, the laser works as a single-pass amplifier. In this region, $s_2=0$; therefore the gain is slightly larger than Eq. (48) suggests. This effect may provide an additional improvement of the efficiency of active unstable resonators that work far from the paraxial regime. In addition, in the paraxial approximation, we do not take into account the increase of the optical path of the signal between reflections for nonparaxial rays, which leads to an increase in the signal intensity. Also, the increase of the size of the output window compared to the paraxial estimate may improve the performance of the device. The effects mentioned may cause an increase in the efficiency compared with the estimates above.

For the parameters of a laser without SHB, see Table 4.

B. Laser with Spatial Hole Burning

The consideration of Subsection 4.A ignores the inhomogeneity of gain caused by the SHB. Now we consider the case with SHB. Assume the reflectivity R of both mirrors to be high (0.95 in the examples considered) and the magnification coefficient to be small (say, less than 1.4). Then the intensities of the counterpropagating waves of the signal are almost equal, and we can use Eqs (44)–(47). We assume some constant pump intensity I_p and calculate $p=I_p/I_{po}$. Using Eq. (47), we obtain

Table 4. Parameters of a Laser without SHB and Examples of Values

Quantity	Expression	Value, Nd:YAG	Value, Yb:YAG
Asymptotic ratio s/p	$\delta_i=\frac{G_0}{G}-1$	7.393	1.855
Saturated absorption	$A=A_0\left(1-\frac{G}{G_0}\right)$	0.936 mm^{-1}	1.419 mm^{-1}
Asymptotic ratio I_s/I_p	$\delta_I=\delta_i\frac{I_{so}}{I_{po}}$	1.644	0.902
Efficiency of pump coupling	$\eta_p=1-\exp(-Ar_2)$	0.846	0.881
Size of pumped spot	$L=\frac{w}{1-\eta_p}$	0.259 mm	0.189 mm
Pump power threshold	$P_{pr}=2hLI_{pr}$	6.704 W	7.919 W
Slope efficiency, direct estimate	$\eta_d=\frac{\delta_I(r_2-r_1)}{2h}$	0.524	0.691
Slope efficiency, independent estimate	$\eta_3=(\lambda_p/\lambda_s)\,\eta_p\,\eta_s$	0.554	0.641
NA of pump suggested	$NA=L/r_2$	0.128	0.125
Beam quality required	$q=\lambda_p/(2nw\mathrm{NA})$	0.044	0.092
Pump intensity profile	$u(r)=\frac{\exp(Ar)r_2}{\{r_2^2+[\exp(2Ar_2)-1]r^2\}^{1/2}}$	$0.76<u<1.05$	$0.67<u<1.03$
NA of signal	$NA_1=(r_2-r_1)/(2Z)$	0.0787	0.1243
NA of signal	$NA_2=L/(2Z)$	0.0852	0.1912
Normalized pump intensity	p (example)	1.000	4.000
Pump intensity	$I_p=pI_{po}$	127.7 W/mm^2	817.9 W/mm^2
Input pump power	$P_{p1}=2LhI_{po}/u_-$	65.391 W	73.678 W
Input pump power	$P_{p2}=2LhI_{po}/u_+$	47.400 W	47.756 W
Normalized signal intensity	$s=\left(\frac{G_0}{G}-1\right)p-\frac{G_0}{G}V-1$	6.393	6.229
Signal intensity	$I_s=sI_{so}$	181.5 W/mm^2	619.2 W/mm^2
Output signal power	$P_s=(r_2-r_1)LI_s$	22.443 W	28.677 W
Local efficiency of medium	$\eta_m=\frac{I_sG}{I_pA}\eta_m=\frac{\lambda_p}{\lambda_s}\frac{1-V/p}{1+U/s}$	0.657	0.767
Local gain (checkback)	$G=G_0\frac{p-V}{1+p+s}$	0.432/mm	1.437/mm
Local absorption (checkback)	$A=A_0\frac{s+U}{1+p+s}$	0.936/mm	1.419/mm
Efficiency, pessimistic estimate	$\eta_-=P_s/P_{p1}$	0.34	0.39
Efficiency, optimistic estimate	$\eta_+=P_s/P_{p2}$	0.47	0.60
Efficiency, independent estimate	$\eta_3=\eta_s\,\eta_p\,\eta_m$	0.48	0.54
Efficiency, balanced estimate	$\eta_4=(\eta_+\eta_-\eta_3)^{1/3}$	0.43 ± 0.05	0.50 ± 0.07

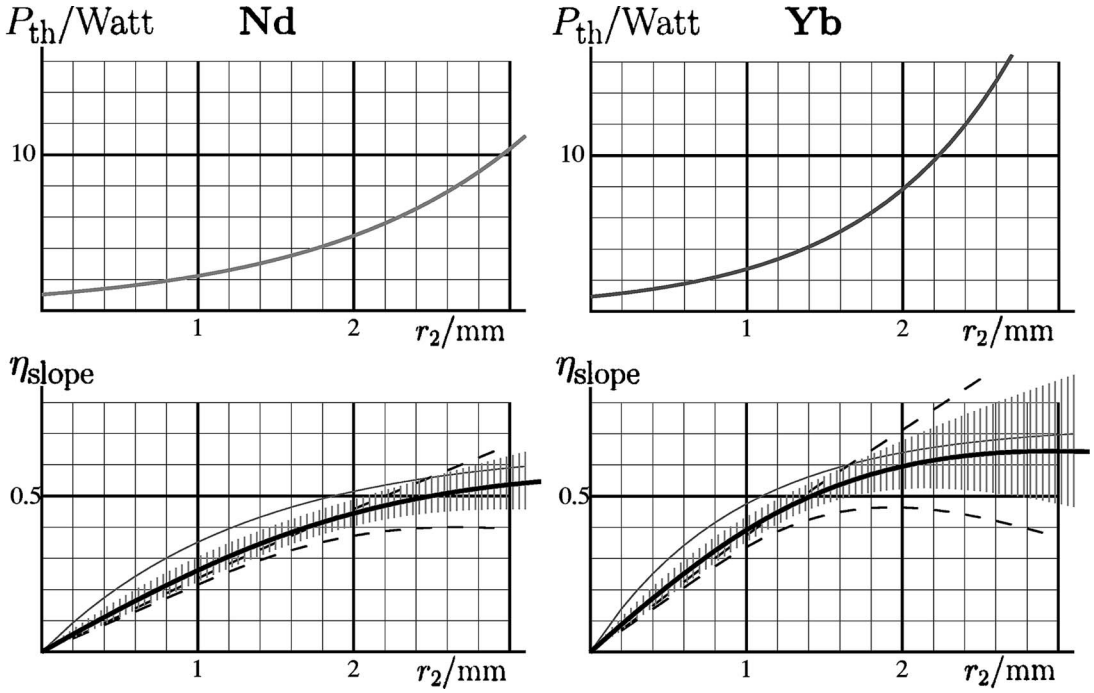

Fig. 8. Pump threshold power P_{pt} for a laser with Nd and a laser with Yb and various estimates of the slope efficiency η_{slope} for the case with SHB: pessimistic and optimistic estimates $\eta_{\pm}=\eta_d u_{\pm}$ are shown with two dashed curves; $\eta_3=(\lambda_s/\lambda_p)\eta_p\eta_s$ is shown with thin solid curves; and the thick curves show the mean geometric values of three estimates. We also plot the corresponding error bars.

$$s=\frac{G_0}{G_1}(p-V)-\frac{1+p}{4}\left\{1+\left[1+8\frac{G_0(p-V)}{G_1(1+p)}\right]^{1/2}\right\}. \quad (58)$$

The gain G_1 should be the same as G by Eq. (48). At $s=0$, Eq. (58) gives the same expression of the threshold pump intensity as Eq. (48). The threshold is plotted in the upper part of Fig. 8. However, the values of this threshold are slightly lower than in Fig. 7 due to the stronger requirements on the pump beam quality discussed below.

Expanding Eq. (58) at large values of p (well above threshold), we obtain the asymptotic estimate of the ratio of the normalized signal intensity to the normalized pump intensity $\delta_i=(s/p)_{\text{asymp}}=G_0/G_1-1/4-1/2[1+8(G_0/G_1)]^{1/2}$. Then, in analogy with Subsection 4.A, we obtain two estimates for the slope efficiency $\eta_{\pm}=\delta_i(I_{\text{so}}/I_{po})(r_2-r_1/2h)u_{\pm}$. These estimates are plotted in lower part of Fig. 8 with the dashed curves.

As in Subsection 4.A, we can also obtain the balanced estimate of the slope efficiency, which we plot in the lower part of Fig. 8. In the same asymptotic case of a strong pump, for the saturated absorption we obtain $A_{\text{asymp}}=A_0\{1-1/\sqrt{[1+2(s/p)_{\text{asymp}}]^{1/2}}\}$. Then the pump absorption efficiency can be estimated as follows: $\eta_{p,\text{asymp}}=1-\exp(-A_{\text{asymp}}r_2)$. For the approximation of constant intensity, we should have the input spot size of pump $L=w/(1-\eta_{p,\text{asymp}})$. This determines the pump power threshold $P_{pt}=2hLI_{pt}$.

Because of the SHB, the NA of the pump should be slightly larger than that in the case without SHB, and the pump intensity threshold happens to be lower than in the case without SHB. The pump power threshold is plotted versus radius r_2 of the device in the upper graphics of Fig. 8 in the same manner as in Fig. 7.

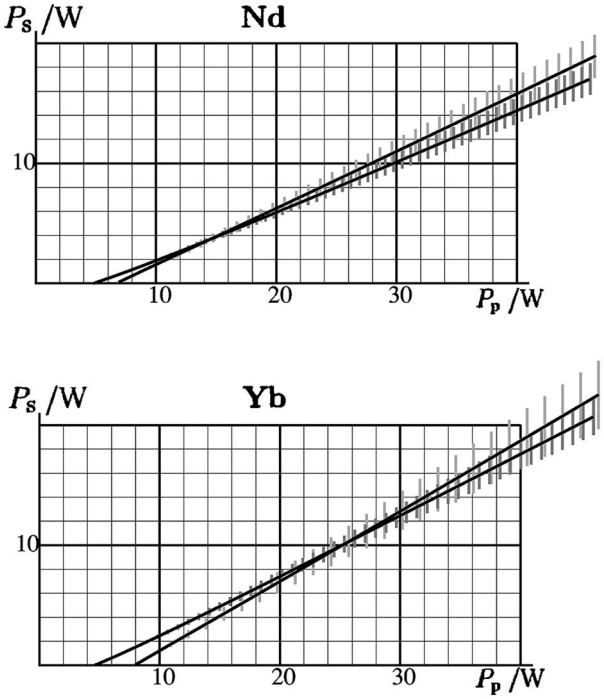

Fig. 9. Output signal power versus input pump power. Lines with a larger tangent correspond to the case without SHB. Lines with a lower tangent correspond to the case with SHB. Here, $r_2=2$ mm, $h=0.75$ mm for Nd, and $r_2=1.6$ mm, $h=0.16$ mm for Yb.

As in the case without SHB we also obtain the balanced estimate $\eta_{3,\text{slope}}=(\lambda_p/\lambda_s)\eta_s\eta_p$ and calculate the mean geo-

Table 5. Parameters of a Laser with SHB and Examples of Values

Quantity	Expression	Value, Nd:YAG	Value, Yb:YAG
Asymptotic ratio s/p	$\delta_i=\frac{G_0}{G}-\frac{1}{4}-\frac{1}{4}\left(1+8\frac{G_0}{G}\right)^{1/2}$	6.079	1.384
Absorption, asymptotic estimate	$A=A_0\left[1-\frac{1}{(1+2\,\delta_i)^{1/2}}\right]$	0.769 mm^{-1}	1.059 mm^{-1}
Slope of intensity	$\delta_I=\delta_i I_{so}/I_{po}$	1.352	0.673
Efficiency of pump coupling	$\eta_p=1-\exp(-Ar_2)$	0.785	0.796
Size of pumped spot	$L=w/(1-\eta_p)$	0.186 mm	0.110 mm
Pump power threshold	$P_{pr}=2hLI_{pr}$	4.807 W	4.614 W
Slope efficiency, direct estimate	$\eta_d=\delta_I(r_2-r_1)/(2h)$	0.431	0.516
Slope efficiency, independent estimate	$\eta_3=(\lambda_p/\lambda_s)\,\eta_p\,\eta_s$	0.515	0.579
NA of pump suggested	$\mathrm{NA}=L/r_2$	0.091	0.072
Beam quality required	$q=\lambda_p/(2nw\mathrm{NA})$	0.062	0.160
Pump intensity profile	$u(r)=\frac{\exp(Ar)r_2}{[r_2^2+(\exp(2Ar_2)-1)r^2]^{1/2}}$	$0.86<u<1.06$	$0.85<u<1.06$
NA of signal	$\mathrm{NA}_1=(r_2-r_1)/(2Z)$	0.0787	0.1243
NA of signal	$\mathrm{NA}_2=L/(2Z)$	0.0611	0.1114
Normalized pump intensity	p (example)	1.000	4.000
Pump intensity	$I_p=pI_{po}$	128 W/mm^2	818 W/mm^2
Input pump power	$P_{p1}=2LhI_{po}/u_{\min}$	41.10 W	33.87 W
Input pump power	$P_{p2}=2LhI_{po}/u_{\max}$	33.43 W	27.14 W
Normalized signal	$s=\frac{G_0}{G}(p-V)-\frac{1+p}{4}\left[1+\left(1+8\frac{G_0}{G}\frac{p-V}{1+p}\right)^{1/2}\right]$	4.953	4.536
Signal intensity	$I_s=sI_{so}$	141 W/mm^2	451 W/mm^2
Output signal power	$P_s=(r_2-r_1)LI_s$	12.47 W	12.17 W
Gain (checkback)	$G_1=\frac{2G_0(p-V)}{1+p+2s+[(1+p)(1+p+2s)]^{1/2}}$	0.432 mm^{-1}	1.437 mm^{-1}
Absorption (checkback)	$A=A_0\left\{1-\frac{1+p-U}{[(1+p)(1+p+2s)]^{1/2}}\right\}$	0.845 mm^{-1}	1.160 mm^{-1}
Local efficiency of medium	$\eta_m=\frac{I_sG}{I_pA}$	0.564	0.683
Efficiency, pessimistic estimate	$\eta_-=P_s/P_{p1}$	0.30	0.36
Efficiency, optimistic estimate	$\eta_+=P_s/P_{p2}$	0.37	0.45
Efficiency, independent estimate	$\eta_3=\eta_s\eta_p\eta_m$	0.38	0.43
Efficiency, balanced estimate	$\eta_4=(\eta_+\eta_-\eta_3)^{1/3}$	0.35 ± 0.03	0.41 ± 0.03
Gain for closest mode	$G_u=\tilde{G}(\lambda_u)$	0.377 mm^{-1}	1.359 mm^{-1}
Gain for closest mode	$G_d=\tilde{G}(\lambda_d)$	0.374 mm^{-1}	1.378 mm^{-1}

metric value (thick curve in the lower part of Fig. 8) and plot the error bars. Combining the analysis of the two subsections, in Fig. 9 we plot the output signal power as a function of the input pump power. We use the value $h=0.75$ mm, $r_2=2$ mm for the case with Nd:YAG and $h=0.16$ mm, $r_2=1.6$ mm for the case with Yd:YAG for two cases without SHB and with SHB.

The smaller absorption in the case with SHB leads to smaller values of size L of the input window, at the same size of the device. For this reason, the threshold power in the case with SHB (Fig. 8) is lower than that in the case without SHB (Fig. 7), but the conditions for the constant pump intensity require higher beam quality of the pump. The resulting slope efficiency happens a little bit lower due to the SHB. However, the difference in the resulting output power (Fig. 9) is not strong.

See Table 5 for the parameters of a laser with SHB.

C. Single-Longitudinal-Mode Operation

We now consider the conditions of the SLM generation. For the SLM operation, the gain of a weak independent field by Eq. (43) should be smaller than G_1 by Eq. (47) for the main signal wave. Wavelengths of the closest modes of the cavity can be expressed as follows:

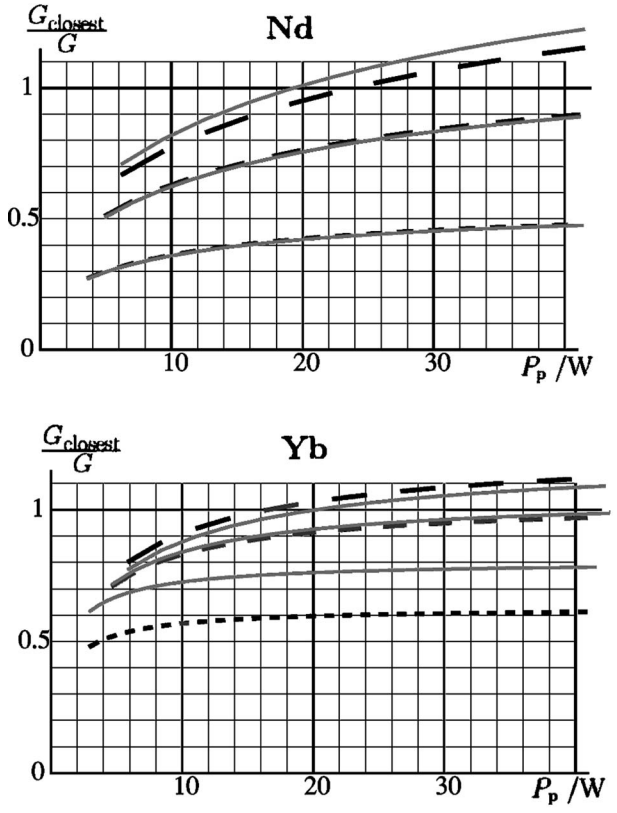

Fig. 10. Relative gain $\tilde{G}/G$ of closest modes by Eqs. (40) and (43) for Nd:YAG and Yb:YAG lasers versus pump power for various values of h. The dashed curves correspond to the highest mode, the solid curves correspond to the lower mode. Case of Nd: $h=1$ mm (upper curves), $h=0.75$ mm (intermediate curves), $h=0.5$ mm (lowest curves). Case of Yb: $h=0.2$ mm (upper curves), $h=0.16$ mm (intermediate curves), $h=0.1$ mm (lowest curves).

$$\lambda_{\pm}=\frac{\lambda_s}{1\pm\lambda_s/(2nh)}. \tag{59}$$

The gain $G_{\pm}=\tilde{G}(\lambda_{\pm})$ for these modes should be compared with the effective gain G_1 of the main mode of the laser; if $G_{\pm}<G_1$, then the single-mode regime is stable. The gain for the closest modes is plotted in Fig. 10 versus input pump power for three values of the cavity length: $h=0.5$, 0.75, and 1 mm for Nd and $h=0.1$, 0.16, and 0.2 mm for Yb.

For Yb:YAG, the length of the cavity could be of the order of $h=0.1$ mm. In the case of Nd:YAG ceramics, $h=0.5$ mm looks reasonable, although a laser with $h=0.7$ mm also may provide the powerful single-mode output at the appropriate adjustment of the pump beam and tuning of the frequency of the main mode. As the relative displacement of mirrors required for such tuning is small (less than a wavelength), it can be performed with pressure on the specimen, as well as with variation of its temperature.

Deviation from the ideal case of uniform intensity does not change the conclusion about high efficiency of the device. The thickness of the specimen (length h of resonator) can be increased while keeping the single-mode operation, if the pump depletes before the seed region. In this case, the stability of such a device becomes dependent on the properties of the pump beam. The application of a special coating[9] mitigates the SHB; this would allow more freedom in the choice of thickness of the sample and slightly increase the efficiency. The question of application of such a coating is rather more economical than physical and falls out of goal of this paper.

Even with simple 95% reflectivity mirrors, the laser with a short unstable cavity may provide single-mode operation with an efficiency of the order of 50%. In the cases of Nd and Yb dopants, the length of the amplifier (thickness of the specimen) should be of the order of 0.5 and 0.1 mm, respectively (Fig. 10); then the threshold is of the order of few watts (Figs. 7–9).

5. CONCLUSIONS

A solid-state laser with a short unstable resonator is suggested (Fig. 1). Such a device allows both extension of transversal size of the thin disk lasers and single-mode operation at high efficiency. The pie-shaped cut should improve the confinement of the pump, but the circular shape of the specimen can also be used (Fig. 2).

The suggested resonator has no need to work in the paraxial regime. Ray tracing (Fig. 3) allows the estimate of the size of the output window in the nonparaxial case (Fig. 4) and shows the limits of the paraxial estimates. The lateral delivery of pump light allows the partial compensation of depletion of pump intensity (Fig. 5). In this case, the pump intensity is almost constant along its propagation in the gain medium. This allows one to obtain high efficiency and simplifies the consideration. Media with Nd and Yb are used as examples to estimate the performance of such a laser in realistic cases. For 95% mirror reflectivity, the slope efficiency can be of the order of 50% with a threshold of a few watts (Fig. 9). The conditions of single-longitudinal-mode operation at high power are realized at a thickness of the specimen of the order of 0.5 mm in the case with Nd:YAG and of the order of 0.1 mm in the case of Yb:YAG (Fig. 10).

The flatness of this device allows efficient heat sink. The large ratio of the volume of the active medium to the length of the resonator can be useful for the generation of high-energy solitary pulses of single-mode light. Such a laser can be used as a source of seed for nuclear fusion drivers and other applications.

ACKNOWLEDGMENT

This work was supported by the 21st Century Center of Excellence program of the Ministry of Education, Science and Culture of Japan. We are grateful to H. Yoneda, M. Musha, and A. Shirakawa for help and discussions.

The e-mail address for D. Kouznetsov is dima@ils.uec.ac.jp.

REFERENCES

1. K. Naito, M. Yamanaka, M. Nakatsuka, T. Kanabe, K. Mima, C. Yamanaka, and S. Naka, "Conceptual design of a laser diode pumped solid state laser system for laser fusion reactor driver," Jpn. J. Appl. Phys. Part 1 **31**, 250–271 (1992).
2. D. B. S. Soh, C. Codemard, S. Wang, J. Nilsson, J. K. Sahu, F. Laurell, V. Philippov, Y. Jeong, C. Alegria, and S. Baek, "A 980-nm Yb-doped fiber MOPA source and its frequency doubling," IEEE Photonics Technol. Lett. **16**, 1032–1034 (2004).
3. H. Liu, S. H. Zhou, and Y. C. Chen. "High-power monolithic unstable-resonator solid-state laser," Opt. Lett. **23**, 451–453 (1998).
4. P. Shi, D. Li, H. Shang, Y. Wang, and K. Du. "An 110 W Nd:YVO_4 slab laser with high beam quality output," Opt. Commun. **229**, 349–354 (2004).
5. J. J. Zaihovski, "Microchip lasers," Opt. Mater. **11**, 255–257 (1999).
6. L. W. Casperson, "Laser power calculation. Sources of error," Appl. Opt. **19**, 422–434 (1980).
7. A. C. Nilsson, E. K. Gustafson, and R. Byer, "Eigenpolarization theory of monolithic nonplanar ring oscillators," IEEE J. Quantum Electron. **25**, 767–790 (1989).
8. D. Shen, C. L. Fincher, D. A. Hinkley, R. A. Chodzoko, T. S. Rose, and R. A. Fields, "Semimonolite Nd:YAG ring resonator for generating cw single-frequency output at 1.06 nm," Opt. Lett. **20**, 1282–1285 (1995).
9. K. Nakagawa, Y. Shimizu, and M. Ohtsu, "High power diode-laser-pumped twisted-mode Nd:YAG laser," IEEE Photonics Technol. Lett. **6**, 499–501 (1994).
10. H. G. Danielmeyer and E. H. Turner, "Electro-optic elimination of spatial hole burning in lasers," Appl. Phys. Lett. **17**, 519–521 (1970).
11. T. Dascalu, T. Taira, and N. Pavel, "100-W quasi-continuous-wave diode radially pumped microchip composite Yb:YAG laser," Opt. Lett. **27**, 1791–1793 (2002).
12. D. Kouznetsov and J. V. Moloney, "Highly efficient, high-gain, short-length, and power-scalable incoherent diode slab-pumped fiber amplifier/laser," IEEE J. Quantum Electron. **39**, 1452–1461 (2003).
13. D. Kouznetsov and J. V. Moloney, "Tapered slab delivery of pump to the double-clad fiber amplifier: analytical approach," IEEE J. Quantum Electron. **40**, 378–383 (2004).
14. P. Kano, D. Kouznetsov, J. V. Moloney, and N. Brio, "Slab delivery of incoherent pump light to double-clad fiber amplifiers: numerical simulations," IEEE J. Quantum Electron. **40**, 1301–1305 (2004).
15. A. Siegman, *Lasers* (University Science, 1986). There is a misprint on p. 875; the ray matrix
$$\begin{bmatrix} 1-2L/R & L \\ 2L/R & 1 \end{bmatrix}$$
should be corrected to
$$\begin{bmatrix} 1-2L/R & L \\ 2/R & 1 \end{bmatrix}$$
.
16. R. Oron, N. Davidson, A. Friesem, and E. Hasman, "Continuous-phase elements can improve laser beam quality," Opt. Lett. **25**, 939–941 (2000).
17. P. C. Becker, N. A. Olsson, and J. R. Simpson, *Erbium-Doped Fiber Amplifiers: Fundamentals and Theory* (Academic, 1999).
18. D. Yu. Kuznetsov, "The transformation of the transverse structure of monochromatic light in the non-linear media," *Optics and Lasers*, V. A. Shcheglov, ed. (Nova Science, 1995).
19. T. Y. Fan, "Optimizing the efficiency and stored energy in quasi-three level lasers," IEEE J. Quantum Electron. **28**, 2692–2697 (1992).